

Monte Carlo simulation of x-ray spectra in diagnostic radiology and mammography using MCNP4C

This content has been downloaded from IOPscience. Please scroll down to see the full text.

2004 Phys. Med. Biol. 49 4897

(<http://iopscience.iop.org/0031-9155/49/21/004>)

View [the table of contents for this issue](#), or go to the [journal homepage](#) for more

Download details:

IP Address: 64.141.84.23

This content was downloaded on 24/11/2014 at 21:44

Please note that [terms and conditions](#) apply.

Monte Carlo simulation of x-ray spectra in diagnostic radiology and mammography using MCNP4C

M R Ay^{1,2}, M Shahriari³, S Sarkar⁴, M Adib⁵ and H Zaidi²

¹ Department of Physics and Nuclear Sciences, AmirKabir University of Technology, Tehran, Iran

² Division of Nuclear Medicine, Geneva University Hospital, 1211 Geneva, Switzerland

³ Department of Nuclear Engineering, Shahid Beheshti University, Tehran, Iran

⁴ Department of Medical Physics, Tehran University of Medical Science, Tehran, Iran

⁵ TPP Co., GE Medical Systems, Iran Authorized Distributor, Tehran, Iran

E-mail: farshid.ay@tppgems.com

Received 16 March 2004

Published 8 October 2004

Online at stacks.iop.org/PMB/49/4897

doi:10.1088/0031-9155/49/21/004

Abstract

The general purpose Monte Carlo N-particle radiation transport computer code (MCNP4C) was used for the simulation of x-ray spectra in diagnostic radiology and mammography. The electrons were transported until they slow down and stop in the target. Both bremsstrahlung and characteristic x-ray production were considered in this work. We focus on the simulation of various target/filter combinations to investigate the effect of tube voltage, target material and filter thickness on x-ray spectra in the diagnostic radiology and mammography energy ranges. The simulated x-ray spectra were compared with experimental measurements and spectra calculated by IPEM report number 78. In addition, the anode heel effect and off-axis x-ray spectra were assessed for different anode angles and target materials and the results were compared with EGS4-based Monte Carlo simulations and measured data. Quantitative evaluation of the differences between our Monte Carlo simulated and comparison spectra was performed using student's *t*-test statistical analysis. Generally, there is a good agreement between the simulated x-ray and comparison spectra, although there are systematic differences between the simulated and reference spectra especially in the K-characteristic x-rays intensity. Nevertheless, no statistically significant differences have been observed between IPEM spectra and the simulated spectra. It has been shown that the difference between MCNP simulated spectra and IPEM spectra in the low energy range is the result of the overestimation of characteristic photons following the normalization procedure. The transmission curves produced by MCNP4C have good agreement with the IPEM report especially for tube voltages of 50 kV and 80 kV. The systematic discrepancy for higher tube voltages is the result of systematic differences between the corresponding spectra.

(Some figures in this article are in colour only in the electronic version)

1. Introduction

Computer simulation of x-ray spectra is one of the most important tools for investigation of patient dose and image quality in diagnostic radiology imaging systems. Early attempts at predicting diagnostic x-ray spectra were undertaken by Kramers (1923). This pioneering work was sustained by several investigators and many research groups are still trying to find an accurate method for computer simulation of x-ray spectra owing to the fact that experimental measurement of x-ray spectra requires special equipment which is available only in a limited number of laboratories (Fewell and Shuping 1978, Fewell *et al* 1981, Laitano *et al* 1991, Antonuk *et al* 1997, Dance *et al* 2000, Wilkinson *et al* 2001). Fewell *et al* measured x-ray spectra with different target/filter combinations for over two decades and have published several measured spectra (Fewell and Shuping 1977, 1978, Fewell *et al* 1981). Since experimental measurement of x-ray spectra is time consuming and remains difficult, different methods for spectra prediction have been presented. These can be divided into three categories: empirical models (Fewell and Shuping 1977, Boone and Seibert 1997, Boone *et al* 1997), semi-empirical models (Birch and Marshall 1979, Boone 1988, Tucker *et al* 1991, Blough *et al* 1998) and Monte Carlo modelling (Kulkarni and Supe 1984, Acosta *et al* 1998, Bhat *et al* 1999, Verhaegen *et al* 1999, Ng *et al* 2000, Ben Omrane *et al* 2003, Verhaegen and Castellano 2002). Although, purely empirical and semi-empirical models remain the fastest methods for x-ray spectra prediction, the models proposed so far still have limitations which prevent their adoption for a large range of applications (Ay *et al* 2004). In addition, most of these models have preset target/filter combinations and thus do not allow investigation of newly developed material compositions on the quality of resulting x-ray spectra. Sophisticated Monte Carlo modelling was adopted as an alternative to overcome the limitations mentioned above. Nevertheless, the prediction of x-ray spectra using the Monte Carlo method is computer intensive and time consuming compared to empirical and semi-empirical models.

The use of the Monte Carlo method to simulate radiation transport has become the most accurate means of predicting the x-ray spectra even in complex geometries owing to more accurate physics modelling and incorporation of appropriate interaction cross section data (Zaidi and Sgouros 2002). Moreover, the method tracks the evolution of all secondary particles (and their descendants) generated by primary electrons. Using the Monte Carlo method, it is possible to transport electrons and photons inside the target and filter to obtain detailed information about the factors contributing to the production of the x-ray spectrum (Acosta *et al* 1998). For the purpose of Monte Carlo simulation of x-ray spectrum, some authors have used self-written or in house developed computer codes (Kulkarni and Supe 1984, O'Meara *et al* 1998), while others have used public domain general-purpose Monte Carlo codes such as EGS4 (Bhat *et al* 1998, 1999, Ben Omrane *et al* 2003), MCNP (Verhaegen *et al* 1999, Mercier *et al* 2000) and ITS (Ng *et al* 2000).

In this work, we used MCNP4C running on Pentium-based PC to simulate the diagnostic radiology and mammography x-ray tube with the aim of predicting the x-ray spectra with different combinations of target/filter such as W/Al, Mo/Mo and Mo/Rh using various tube voltages (between 50 and 140 kV in diagnostic radiology and 30 kV in mammography) and different anode angles (between 6° and 18°). The Be window and air between tube window and measurement point were simulated. This paper addresses particularly some aspects not sufficiently covered in previously published papers, namely the variation of the radiation output across the x-ray beam, the anode heel effect and off-axis spectra for different target angles both in diagnostic radiology and mammography. The main motivations behind the choice of this code are its wide use by the medical physics community, wide acceptance

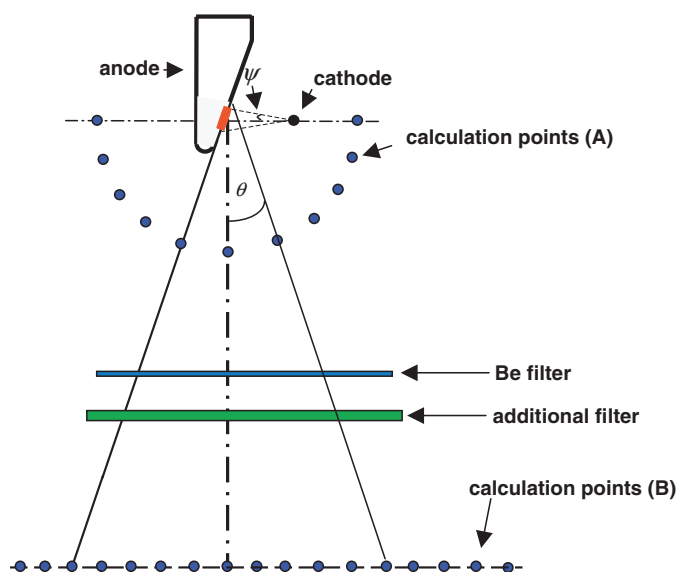


Figure 1. Geometry of the experimental set-up used for Monte Carlo simulation of x-ray spectra and assessment of anode heel effect. The position of detectors for calculation of exposure around the target (A) and anode heel (B) is also shown.

as an international standard for coupled particle transport having the best condensed history electron physics package and remarkable tally capabilities in addition to a powerful reporting system of statistical checks (Briesmeister 2000, Mercier *et al* 2000). The validity of MCNP4C simulated data was checked by comparing the calculated spectra, transmission curves and heel effect with the IPEM report number 78 (Cranley *et al* 1997), measured data (Fewell *et al* 1981, Bhat *et al* 1998, 1999, Pernieka *et al* 1997) and EGS4-based Monte Carlo simulations (Bhat *et al* 1999), respectively.

2. Material and methods

2.1. The MCNP4C code

MCNP is a general-purpose Monte Carlo code that can be used for neutron, photon and electron or coupled neutron/photon/electron transport (Briesmeister 2000). The code treats an arbitrary three-dimensional configuration of materials in geometric cells bounded by first and second degree surfaces and fourth degree elliptical tori. For photons transport, the code takes into account incoherent and coherent scattering, the possibility of fluorescent emission after photoelectric absorption and bremsstrahlung. The continuous slowing down approximation energy loss model is used for electron transport. To follow an electron through a significant energy loss, the MCNP4C code breaks the electron's path into many steps. These steps are chosen to be long enough to encompass many collisions (so that multiple scattering theories are valid) but short enough so that the mean energy loss in any one step is small (so that the approximations necessary for multiple scattering theories are satisfied). Except for the energy loss and straggling calculation, the detailed simulation of the electron history takes place in the sampling of the substeps. The Goudsmit–Saunderson theory is used to sample from the distribution of angular deflections, so that the direction of the electron can change at the end of each substep. For electron transport, MCNP addresses the sampling of bremsstrahlung photons at each electron substep. The table of production probabilities is used

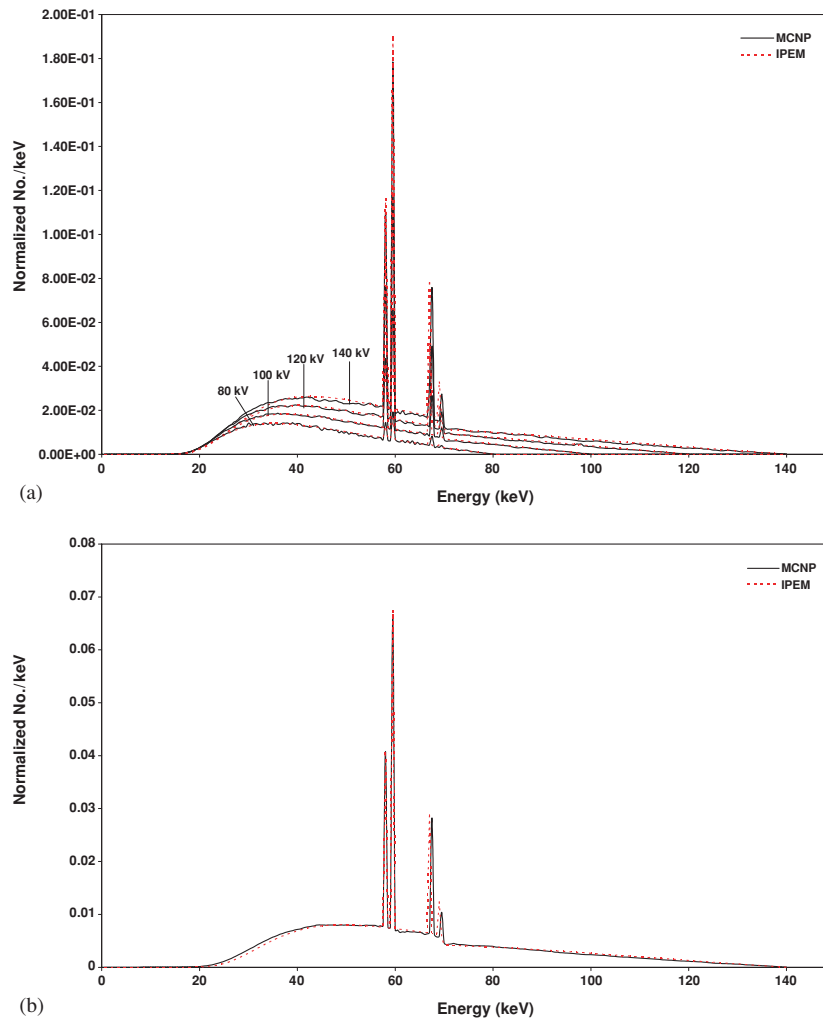


Figure 2. (a) Comparison of x-ray spectra produced by MCNP4C and IPEM report 78 for various tube voltages. (b) Same as (a) for 140 kV tube voltage with 0.1 mm Cu additional filter.

to determine whether a bremsstrahlung photon will be created (Hughes 1997). To improve the efficiency of electron and photon transport, two cards (PHYS:P and PHYS:E) are implemented in MCNP for biasing some physical parameters such as production of secondary electrons by photons (IDES), coherent scattering (NOCOH), bremsstrahlung angular distribution (IBAD) and production of characteristic x-rays (XNUM). The default value for the latter ($XNUM = 1$) results in the analog number of tracks being sampled. If $XNUM > 0$, the number of photons produced is $XNUM$ times the number that would be produced in the analog case, and a corresponding weight adjustment is made. Setting $XNUM$ to zero turns off the production of x-ray photons by electrons.

2.2. Simulation of x-ray spectra using MCNP4C

The procedure of x-ray production consists of tracking a large number of electrons incident on the target until they are absorbed or emerge from it, and calculating the number of

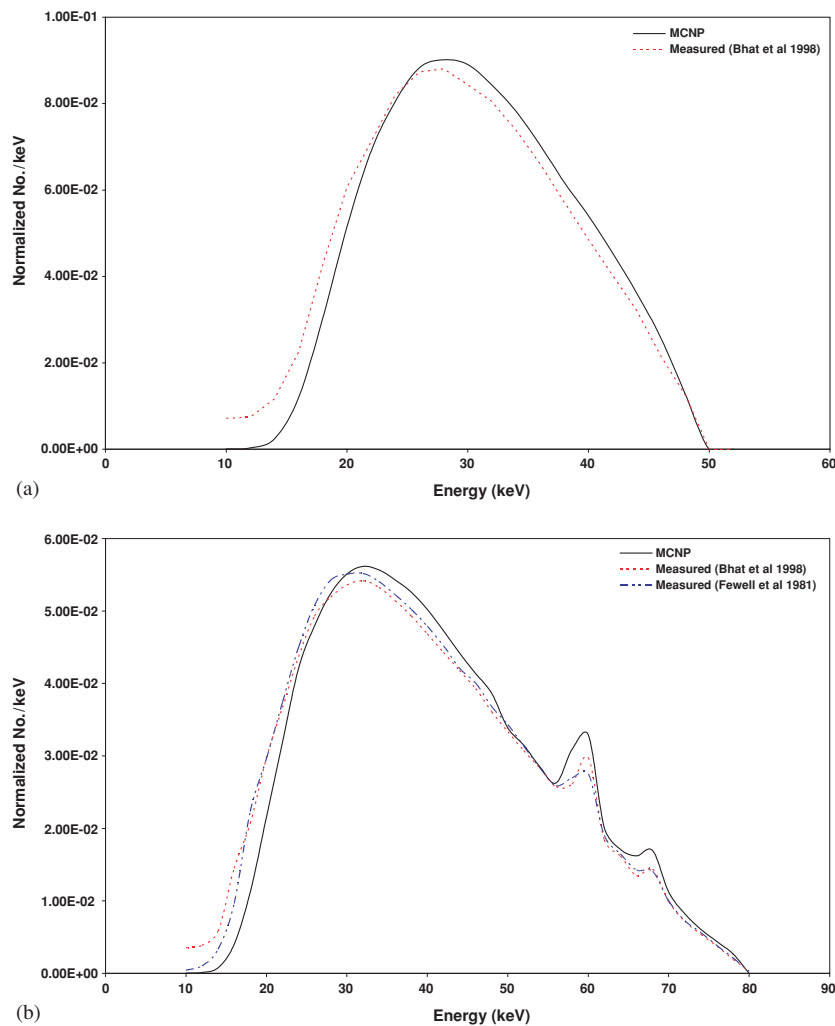


Figure 3. Comparison of x-ray spectra for various tube voltages produced by MCNP4C and measured data by Fewell *et al* (1981) and Bhat *et al* (1998). (a) 50 kV, (b) 80 kV, (c) 100 kV.

bremstrahlung and characteristic photons produced by them during their travel within the target (Kulkarni and Supe 1984). For simulation of x-ray spectra, MCNP4C was run in photon and electron mode (mode: P, E) using default values for PHYS:P and PHYS:E cards to enable full electron and photon transport (XNUM was modified in our experiments to investigate the intensity of produced characteristic photons).

The procedure starts with definition of an electron source (defined in our experiments as a point source) emitting the electrons with energy E within a solid angle ψ towards the target. The focal spot size on the target can be adjusted by changing this angle. Focal spot sizes of 0.3, 0.6 and 1.2 mm corresponding to the projection on the beam central axis of the large diameter of the ellipse covered by solid angle ψ on the target were investigated. Although the approximation of the focal spot shape by an ellipse is a rough estimation, it was considered reliable for the assessment of the influence of focal size on heel effect.

We have considered a constant energy for emitted electrons in most of the cases, although the effect of ripple in electrons energy was simulated in one experiment to study its effect on

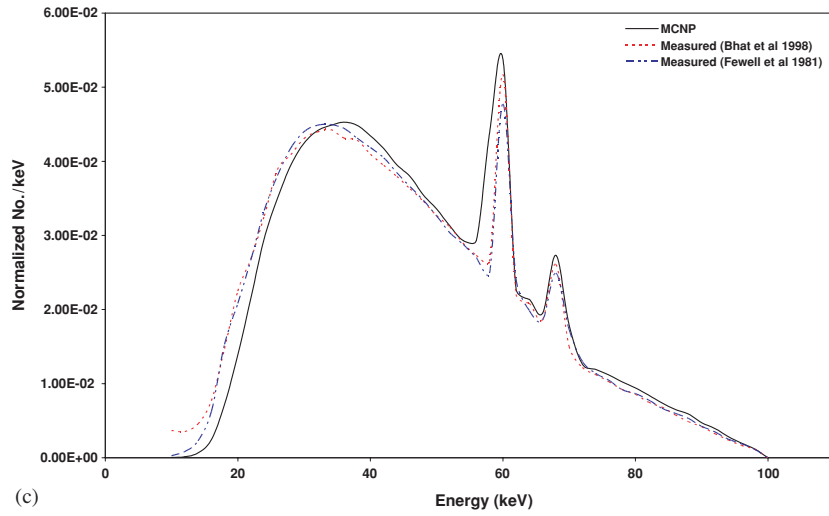


Figure 3. (Continued.)

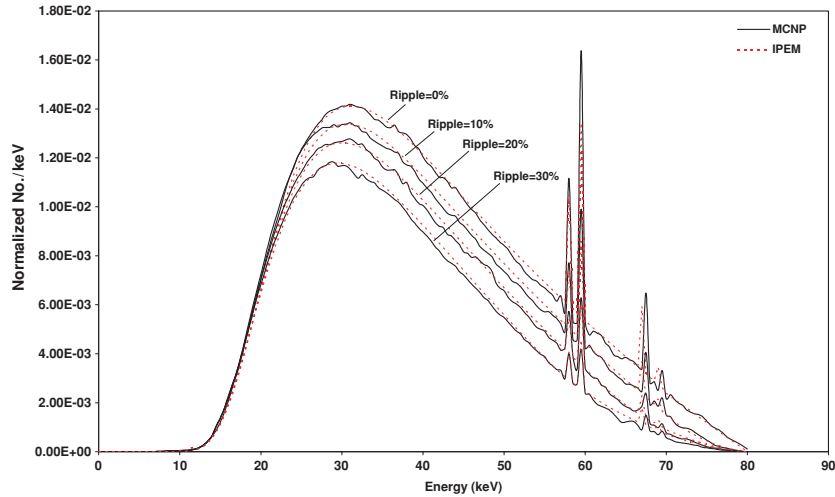


Figure 4. Comparison of x-ray spectra using various tube voltage ripple factors in 80 kV produced by MCNP4C and IPEM report 78.

the calculated spectra. To simulate ripple in MCNP4C, we used the following formulation for ripple factor and tube voltage (Boone and Seibert 1997):

$$\text{Ripple factor (RF)} = 100 \times \frac{kV_{\max} - kV_{\min}}{kV_{\max}}. \quad (1)$$

Thus, the energy of an electron before emission towards the target is sampled uniformly from tube voltage waveform with different ripple values:

$$kV(t) = kV_{\max} \left[1 - \frac{\text{RF}}{100} (1 - |\sin(\omega t)|) \right] \quad (2)$$

where t is time. When the ripple is neglected (i.e. $\text{RF} = 0$), $kV_{\max} = kV$.

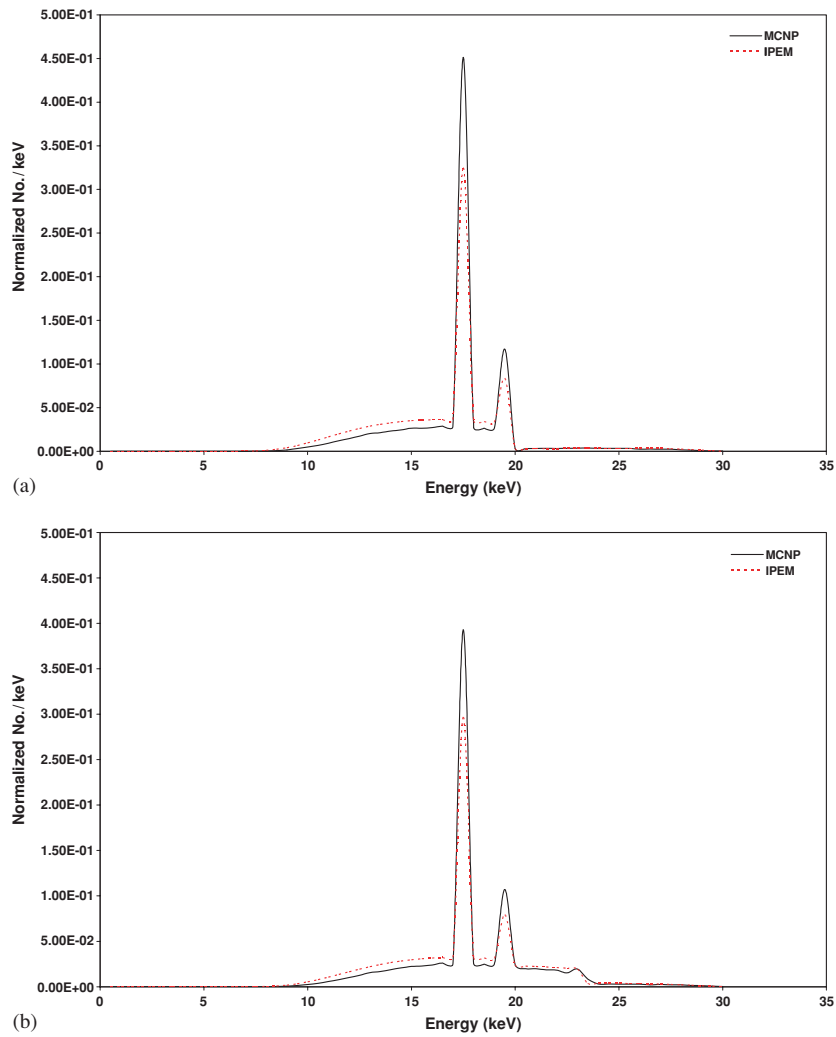


Figure 5. Comparison of 30 kV x-ray spectra produced by MCNP4C and IPEM report 78 for (a) Mo target with 0.5 mm Be and 0.03 mm Mo filter, (b) Mo target with 0.5 mm Be and 0.025 mm Rh and (c) W target with 0.5 mm Be and 1.2 mm Al.

When the electrons strike the target, the code transports the electrons inside the target material until they are stopped after losing their kinetic energy. During the electrons' transport, all bremsstrahlung and characteristic x-ray production is considered. The calculated spectrum is then normalized to the total number of photons in the spectrum. The experimental set-up used in our simulation was based on the RAD 60 x-ray tube (Varian Medical Systems, CA) material composition and target dimensions (figure 1).

MCNP4C simulations without applying variance reduction techniques require an unacceptably long time to produce statistically relevant results. Thus, a variance reduction technique known as point detector (F5 tally), belonging to the class of partially-deterministic variance reduction methods implemented in MCNP4C was used. In this method, the transport of particles towards the detector is replaced by a deterministic estimate of potential contribution to the detector (Briesmeister 2000). The point detector tally measures photon flux at a point

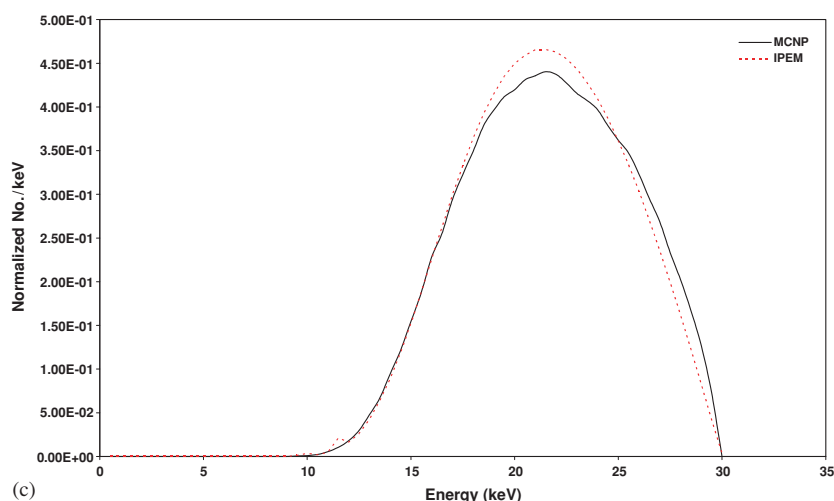


Figure 5. (Continued.)

(unit is photons cm^{-2} or MeV cm^{-2}), which is normalized to be per starting particle. We used the unit photons cm^{-2} for spectra generation and MeV cm^{-2} for exposure assessment in the part related to investigation of anode heel effect. The point detectors were arranged in the calculation points *A* and *B* shown in figure 1 to calculate the exposure around the target and study anode heel effect. Note that the arrangement of point detectors for the calculation of exposure in the axis perpendicular to the anode–cathode axis is not shown. According to the MCNP user manual (Briesmeister 2000), an uncertainty of less than 5% is required for point detector tally (F5) to produce a generally reliable confidence interval. The maximum uncertainty regarding the number of produced photons within each energy bin of widths 0.5, 1 and 2 keV is less than 2% in our simulations, the magnitude of which depends on the number of simulated electrons (in our case 4×10^7).

The x-ray beam is produced as electrons slow down in the anode and encounter some attenuation in the anode material depending on the anode angle and the beam direction. The x-rays propagate isotropically from the point of production, but the direction towards the Be window is the only one of interest for measurement of the x-ray spectra. After passing through the Be window, the x-ray spectrum passes through the additional filter material and air for further attenuation of the x-ray beam before the measurement point. Table 1 summarizes all the x-ray tube parameters investigated in the experiments carried out in this work. The simulated x-ray spectra using MCNP4C were compared with experimental measurements and spectra calculated by IPEM report number 78 described below. The comparative assessment encompassed calculation of transmission curves based on both computational models. The calculation of transmission curves involved running the code for different thicknesses of aluminium filter incrementing in 1 mm steps in radiology and 0.1 mm in mammography. To convert the photon spectra to kerma in air, the total number of transmitted photons in each energy bin for each thickness was multiplied by a related photon to kerma conversion factor (ICRU 1989) and then normalized relative to the air kerma without the filter being present.

Quantitative evaluation of the differences between Monte Carlo simulated and calculated spectra was performed using statistical analysis. The student's *t*-test values and the corresponding significance levels associated with the student's analysis (two-tailed test)

Table 1. Summary of x-ray tube parameters investigated in this work using MCNP4C-based Monte Carlo simulations.

Figure	Tube voltage (kV)	Target/Angle	Filter (mm)	FSD ^a (mm)
2a ^b	80–140	W/12°	1 Be/2.5 Al	750
2b ^b	140	W/12°	1 Be/2.5 Al/0.1 Cu	750
3a ^b	50	W/12°	1.2 Al	3500
3b ^b	80	W/12°	1.2 Al	3500
3c ^b	100	W/12°	1.2 Al	3500
4 ^b	80 (ripple 0–30%)	W/12°	1.2 Al	750
5a ^b	30	Mo/10°	0.5 Be/0.03 Mo	500
5b ^b	30	Mo/10°	0.5 Be/0.025 Rh	500
5c ^b	30	W/14°	0.5 Be/1.2 Al	750
6a,b ^b	30	Mo/10°	0.5 Be/0.03 Mo	500
7a ^c	50–140	W/12°	1.2 Al/0–20 Al	750
7b ^c	30	Mo/12°	1 Be/0.035 Mo/0–2 Al	500
8a,b,c ^b	100	W/12°	1.2 Al	3500
9a,b,c ^b	100	W/6°–14°	1.2 Al	750
10a ^d	100	W/12°	1.2 Al	3500
10b ^d	100	W/12°	1.2 Al	200
10c ^d	100	W/8°–12°	1.2 Al	750
11a ^d	80–140	W/6°–18°	1 Be/2.5 Al	750
11b ^d	25–35	Mo/6°–18°	0.5 Be/0.03 Mo	1000

^a Distance between focal spot and measurement point.

^b X-ray spectrum data.

^c Transmission curve data.

^d Radiation intensity data.

were calculated for the MCNP4C simulated spectra as compared to the IPEM report and experimental measurements. If the calculated *t*-value is greater than the critical *t*-value, the null hypothesis of no statistically significant difference (at the 95% confidence level) is rejected. It is worth pointing out that failure to prove statistically significant differences is not sufficient to confirm that the results are statistically identical. Generally, the paired *t*-test showed no statistically significant differences between the MCNP and IPEM spectra for all experiments performed in this work.

One unfortunate consequence of the line-focus principle is that the radiation intensity on the cathode side of the x-ray field is higher than that on the anode side. The intensity distribution falling on a plane at right angles on the axis of the window (e.g., a film or a screen) is not uniform owing to the anode heel effect (Bushong 1998). In our experiments, the anode heel effect and off-axis x-ray spectra were assessed for different anode angles and target materials and the results were compared with EGS4-based Monte Carlo simulations and measured data published by Bhat *et al* (1999).

2.3. IPEM report no. 78

The original version of the catalogue based on a semi-empirical model for computing x-ray spectra (Birch and Marshall 1979) was published in 1979 and provided essential data useful for applications in diagnostic radiology and mammography (Birch *et al* 1979). The current electronic version (Cranley *et al* 1997) contains sets of radiology and mammography x-ray spectra with much wider ranges than the previous version. This version uses the XCOM photon cross section library (Berger and Hubbell 1987) to calculate linear attenuation coefficients of various materials. The unattenuated photon spectra are given for tungsten targets, tube potential

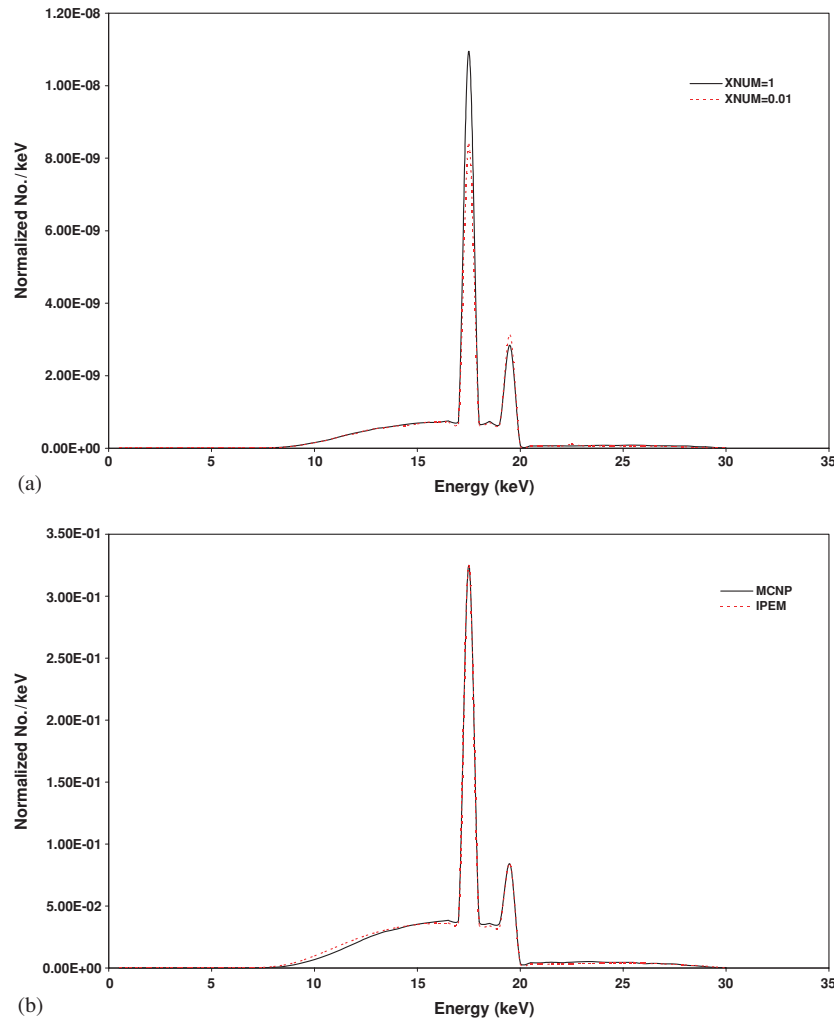


Figure 6. (a) Plots of 30 kV x-ray spectra simulated by MCNP4C for Mo target with 0.5 mm Be and 0.03 mm Mo filter produced for XNUM = 1 and 0.01. (b) Comparison between x-ray spectra produced by MCNP4C with XNUM = 1 and IPEM report 78 after manual setting of the intensity of characteristic photons in the MCNP4C spectra to match the value computed by IPEM.

from 30 kV to 150 kV, and target angles from 6° to 22° . The ripple value can be changed from 0 to 30%. Constant potential mammographic spectra are provided from 25 kV to 32 kV for molybdenum and rhodium targets for target angles ranging between 9° and 23° . All spectra are provided at energy bin width of 0.5 keV (Cranley *et al* 1997). The IPEM report 78 was used as reference to compare with the MCNP simulations because of its popularity and wide availability (Ng *et al* 2000).

3. Results and discussion

3.1. X-ray spectra in diagnostic radiology and mammography

One of the most important parameters influencing the quality of the x-ray spectrum is filtration. The produced x-ray beam after attenuation in the target passes through the

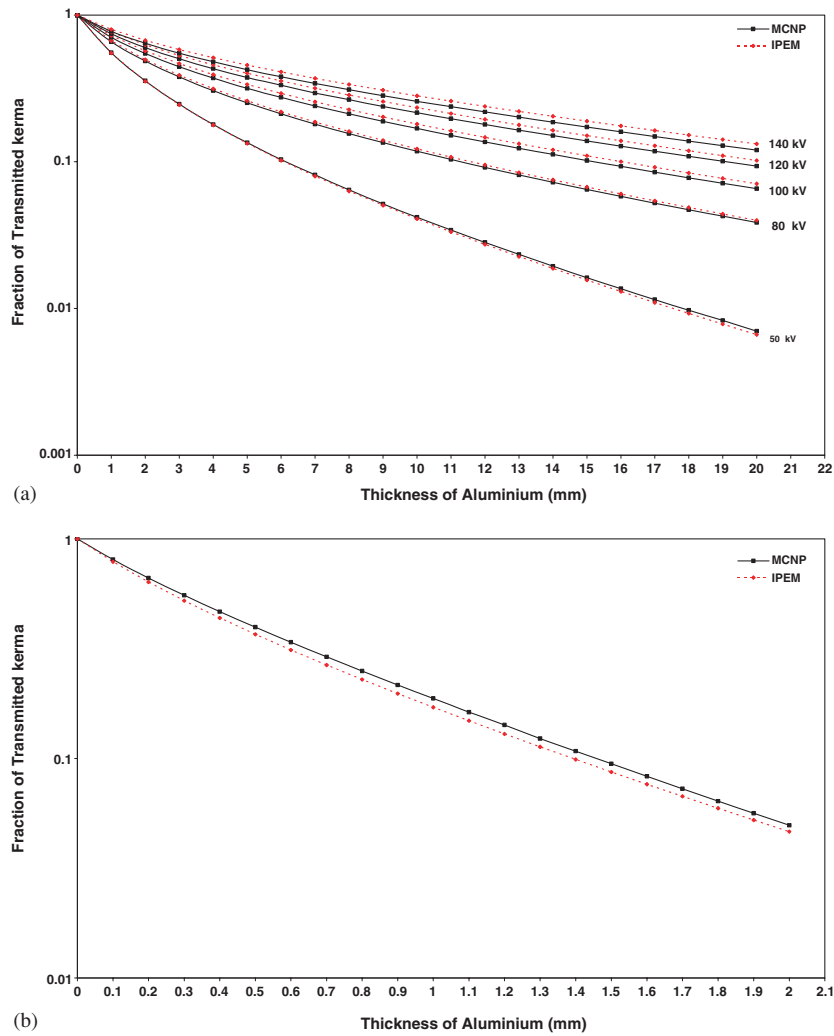


Figure 7. Comparison of transmission curves produced by MCNP4C and IPEM report 78 for (a) tungsten target between 50 and 140 kV and (b) molybdenum target at 30 kV.

tube’s inherent filtration (e.g., Be window) and other filter materials (e.g., aluminium for the attenuation of soft x-rays). Figure 2(a) shows simulated x-ray spectra according to the set-up summarized in table 1 for different tube voltages and their comparison with IPEM report no. 78. The uncertainty achieved in figure 2(a) by simulating 4×10^7 electrons is $\sim 2\%$ and this value decreases to $\sim 1\%$ in figure 2(b) by simulating 1×10^8 electrons. Figure 2(b) shows the simulated x-ray spectrum and its comparison with the IPEM report no.78 for 140 kV tube voltage using a different filter combination, namely 2.5 mm Al, 1 mm Be and 0.1 mm Cu additional filter.

The x-ray spectrum shows significant tungsten *K* x-rays at 58, 59.5, 67.5 and 69 keV, the small shift in characteristic x-ray energy being the result of binning the data into 0.5 keV energy intervals. It can be seen that our results have good agreement with the IPEM report with small differences visible in the intensity of characteristic x-rays and the low energy range, namely between 20 and 40 keV. The intensity of $K_{\alpha 1}$ (59 keV) and $K_{\alpha 2}$ (58 keV) x-ray production by

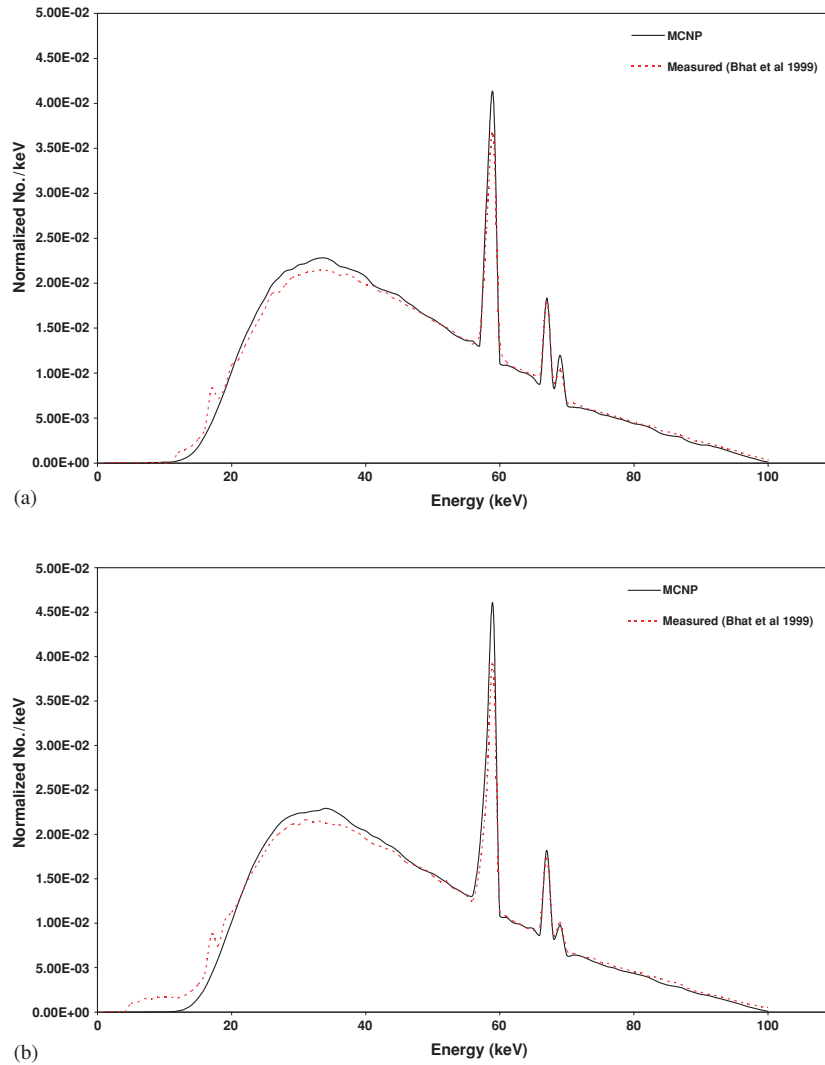


Figure 8. Comparison of simulated and measured on- and off-axis x-ray spectra for 100 kV tube voltage. (a) Central axis, (b) 6° cathode side and (c) 6° anode side.

MCNP4C is slightly higher than IPEM in tube voltages lower than 100 kV and this behaviour is reversed for tube voltages greater than 100 kV while the intensity of $K_{\beta 1}$ (67 keV) and $K_{\beta 2}$ (69 keV) characteristic photon production by IPEM is higher than MCNP4C for all tube voltages. This is consistent with the observations made by Verhaegen *et al* (1999) using the previous version of the code (MCNP4B). Characteristic photons in MCNP are created by the electron impact ionization (EII) process. However, the model overestimates the total number of EII characteristic photons especially in the mammography energy range. This is regulated by the parameter XNUM on the PHYS:E card, which is used to control the sampling of x-ray photons produced along electron substeps.

Figure 3 compares simulated spectra (2 keV energy bin) with experimental spectra published by Fewell *et al* (1981) and Bhat *et al* (1998) for different tube voltages. The simulated spectra have higher intensity in characteristic x-rays for the reasons mentioned

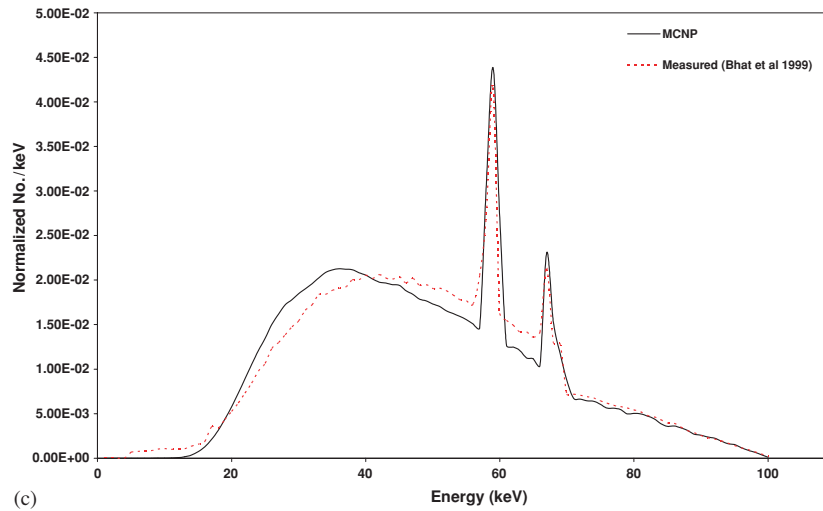


Figure 8. (Continued.)

above. Note that a pure tungsten target was used in our simulation, while the targets used in the experimental measurements have some rhenium and molybdenum impurity. It is worth emphasizing that both el03 and el1 treatments only take into account the highest Z component of the material for production of k-shell x-rays in MCNP (Briesmeister 2000). Thus, the tungsten k-shell masks the x-ray characteristic of added low Z impurities. Figure 4 shows the effect of tube voltage ripple on production of simulated x-ray spectra and its comparison with IPEM report no. 78. Some authors modelled the tube voltage ripple by combining a number of spectra generated at different constant tube potentials, each one being weighted according to the time for which that tube potential occurs (Boone and Seibert 1997, Cranley *et al* 1997). In our experiments, we modelled the tube voltage ripple during Monte Carlo simulation of x-ray spectra by uniformly sampling from the tube voltage waveform (equation (2)). Similar to the results reported above, there is good agreement between simulated and calculated spectra apart from the small shift in characteristic photon energy for the reasons explained above. A 30% ripple is probably higher than most inverter generators as most of them produce ripple factors between 5% and 15% (Boone and Seibert 1997).

Comparisons of the simulated x-ray spectra using MCNP4C with IPEM report 78 for different target/filter material combinations including molybdenum and tungsten as targets and molybdenum, rhodium and aluminium as filters are shown in figure 5. Although there are no statistically significant differences between MCNP4C and IPEM data in Mo target material, the low energy x-ray (<19.5 keV) intensity calculated by IPEM is higher than MCNP4C, which is again the result of the significant overestimation of the intensity of characteristic x-rays in MCNP4C following the normalization procedure. The same observations were reported by Wilkinson *et al* (2001), where the characteristic x-rays in their measured spectrum at 20 keV had a higher intensity in comparison with the IPEM model predictions.

Figure 5(b) shows that the rhodium filter transmits more bremsstrahlung radiation than the Mo filter especially for energies greater than 20 keV, because the attenuation of the Rh filter in this energy range is lower than the attenuation of the Mo filter. Figure 5(c) shows the tungsten target spectra where the spectrum generated by MCNP4C has good agreement with IPEM in the energy range <17 keV, but the intensity of the spectrum in the energy range 17–25 keV is lower than IPEM. This behaviour is reversed for energies >25 keV.

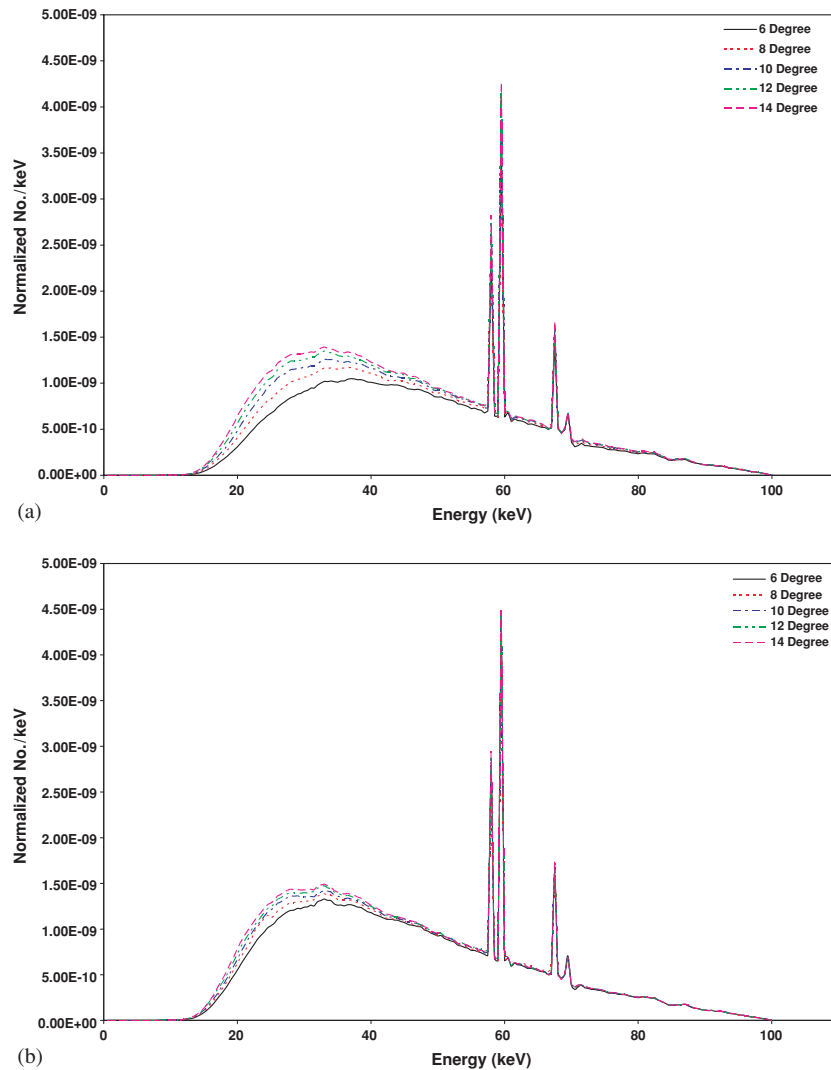


Figure 9. Simulated x-ray spectra for 140 kV tube voltage for various target angles. (a) Central axis. (b) 6° cathode side. (c) 6° anode side.

The optimal adjustment of the XNUM parameters in the PHYS:E card to reduce the intensity of characteristic x-ray production proved to be a difficult issue. Figure 6(a) shows the difference between the simulated spectra with different values of XNUM (1 and 0.01) with the set-up used in figure 5(a). It can be shown that the difference between MCNP simulated spectra and IPEM spectra in the low energy range (figures 5(a) and (b)) is the result of the overestimation of characteristic photons following the normalization procedure. Good agreement between the spectra has been achieved (figure 6(b)) after manual adjustment of the characteristic x-ray intensity in the MCNP spectrum (XNUM = 1) to match the value of the IPEM spectra.

The difference in the quality of x-ray spectra produced by MCNP4C and IPEM report no.78 is further illustrated in figure 7 which shows the transmission curves through an aluminium filter computed from various spectra in increments of 1 mm in diagnostic radiology

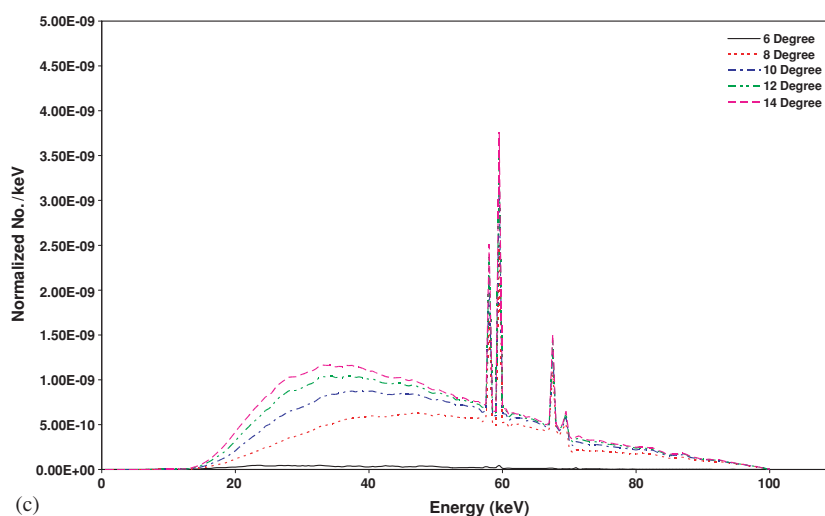


Figure 9. (Continued.)

Table 2. Comparison between measured, calculated (IPEM report 78) and simulated (MCNP4C) HVLs and mean spectrum energy for spectra produced using 12° target angle and different tube voltages. The percentage difference between IPEM and MCNP4C estimates is also shown.

kV	Target material	Filter (mm)	Mean spectrum energy (keV)			First HVL (mm Al)				
			IPEM	MCNP	Diff (%)	Bhat (1998)	Fewell (1981)	IPEM	MCNP	Diff (%)
30	Mo	0.5 Be 0.035 Mo	16.8	17.0	-1.2	-	-	0.32	0.35	-9.4
50	W	1.2 Al	29.9	29.4	+1.7	1.32	-	1.19	1.18	+0.8
80	W	1.2 Al	40.5	40.4	+0.3	1.80	1.81	1.97	1.95	+1.0
100	W	1.2 Al	46.9	46.2	+1.5	2.35	2.29	2.64	2.51	+4.9
120	W	1.2 Al	52.6	51.6	+1.9	-	-	3.38	3.17	+6.2
140	W	1.2 Al	57.4	56.3	+1.9	-	-	4.19	3.75	+10.5

and 0.1 mm in mammography. The transmission curves produced by MCNP4C have good agreement with the IPEM report especially for tube voltages of 50 kV and 80 kV. The systematic discrepancy for higher tube voltages is the result of systematic differences between the corresponding spectra (figure 2). The average and maximum differences in transmission curves for energies between 50 and 140 kV (five energies) are -2.7, 3.2, 6, 6.7, 7.31% and -5.9, 3.8, 7.5, 8.4, 9.2%, respectively (figure 7(a)).

Table 2 compares the mean spectrum energy and HVL for different tube voltages as measured by physical experiments and calculated using IPEM and MCNP4C spectra. The percentage differences vary between -1.2% to 1.9% and -9.4% to 10.5% for mean spectrum energy and HVLs, respectively, for all tube voltages and targets/filters investigated. The results indicate that the percentage difference between HVLs calculated from MCNP4C spectra and IPEM spectra increases with increasing tube voltage. Moreover, the mean energy of IPEM spectra in the diagnostic radiology energy range is higher than spectra calculated by MCNP4C. The amplitude of this difference increases with increasing tube voltage, thus increasing the differences between transmission curves. The higher quality of IPEM spectra for tube voltages

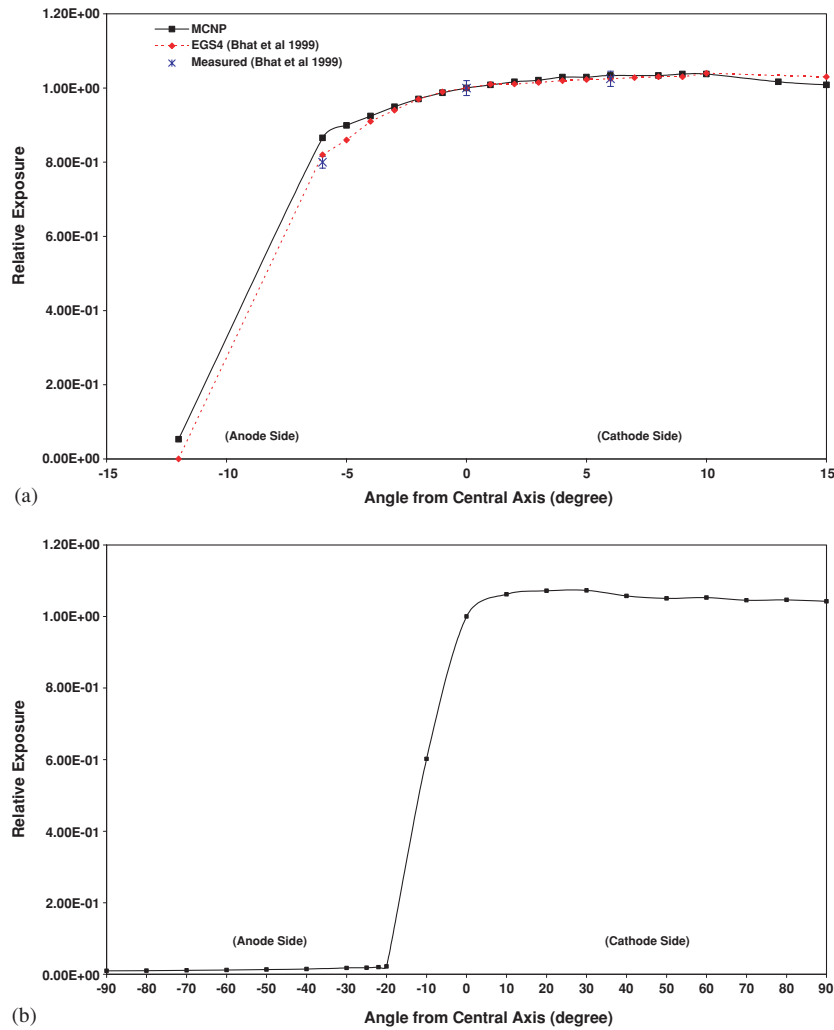


Figure 10. (a) Comparison of simulated and measured relative exposure values in different directions relative to the central axis (calculation points B in figure 1). (b) Relative exposure around the target (calculation points A in figure 1). (c) Normalized exposure on the axis perpendicular to the anode–cathode axis.

higher than 80 kV induces higher values in transmission curves in comparison with MCNP4C spectra.

In our simulation of x-ray spectra resulting from the use of different target/filter combinations in mammography, the tube voltage was assumed to be 30 kV. The transmission curve for the spectrum produced from a molybdenum target with 1 mm Be and 0.035 mm Mo additional filter was calculated. An uncertainty of 0.6% was reached by simulating 3×10^7 electrons. In the mammography energy range, the quality of MCNP4C spectra is higher than IPEM, thus the IPEM transmission curves have lower values compared to those estimated by MCNP4C. The average and maximum differences observed are -7.6% and -9.8% at tube voltage 30 kV in mammography (figure 7(b)). To further investigate the validity of our simulation results, we compared our calculated HVL with measured data published by the

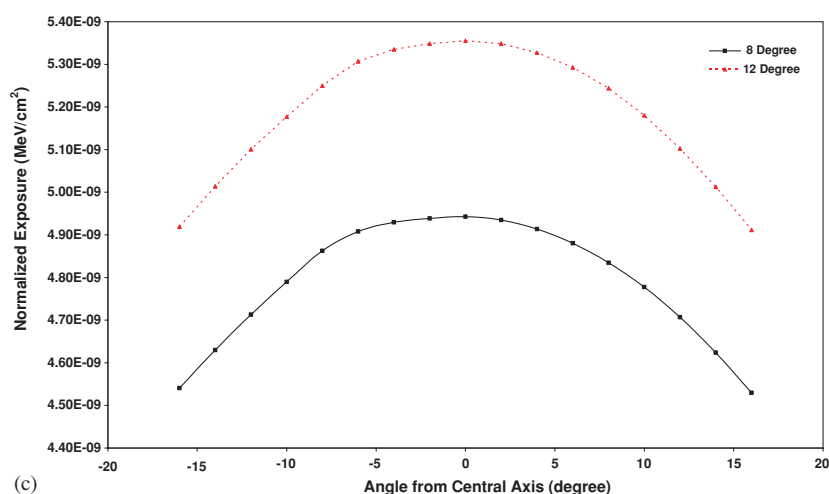


Figure 10. (Continued.)

SSDL laboratory of the IAEA (Pernieka *et al* 1997). They reported 0.348 mm Al for first HVL while we calculated 0.35 mm (-0.6% difference). Note that there are some differences between their experimental set-up (0.8 mm Be filter, 0.03 mm Mo filter, 20° Mo target angle) and our simulation set-up (1 mm Be filter, 0.035 mm Mo filter, 12° Mo target angle). According to our estimation, the 8° difference in target angle produces 3.8% difference in the first HVL.

3.2. Assessment of anode heel effect in diagnostic radiology and mammography

Figure 8 shows the on- and off-axis spectra for a tungsten target at 6° anode side and 6° cathode side and compares them with experimental measurements (Bhat *et al* 1999). The shape of the anode side spectrum after passing through the target skewed towards the higher energy with some distortion in the characteristic tungsten x-ray at 69.5 keV (figure 8(c)). Figure 9 shows the central axis and off-axis x-ray spectra for different target angles. The anode side spectrum encounters more attenuation when using small target angles while the cathode side spectra are approximately similar for all target angles except for a slightly higher attenuation for small target angles in the low energy range.

Figure 10(a) shows the variation of relative exposure with respect to the central axis (calculation points B in figure 1) as simulated by the MCNP4C code and compares it with experimental measurements and EGS4-based Monte Carlo simulations published by Bhat *et al* (1999). The average difference between EGS4 and MCNP simulations for 18 different angles is 0.8% . The maximum difference is -5.5% at 6° anode side, while the maximum difference between MCNP and measured data is -8.2% in the same position. Generally there is good agreement between the relative exposure estimated by MCNP, EGS4 and the experimental data on the cathode side. A small discrepancy (-1.6%) is, however, visible starting from 4° anode side due in our opinion to differences in target dimensions used in both experiments. The radiation escaping from the x-ray tube housing through areas other than the desired x-ray window increases the dose to the patient and surroundings. Figure 10(b) shows the relative exposure around the target at distance 200 mm from the focal spot, which is useful for calculation of x-ray tube shielding. The exposure has been calculated after attenuation of produced x-ray spectra by a 1.2 mm Al filter (calculation points A in figure 1). Obviously, the

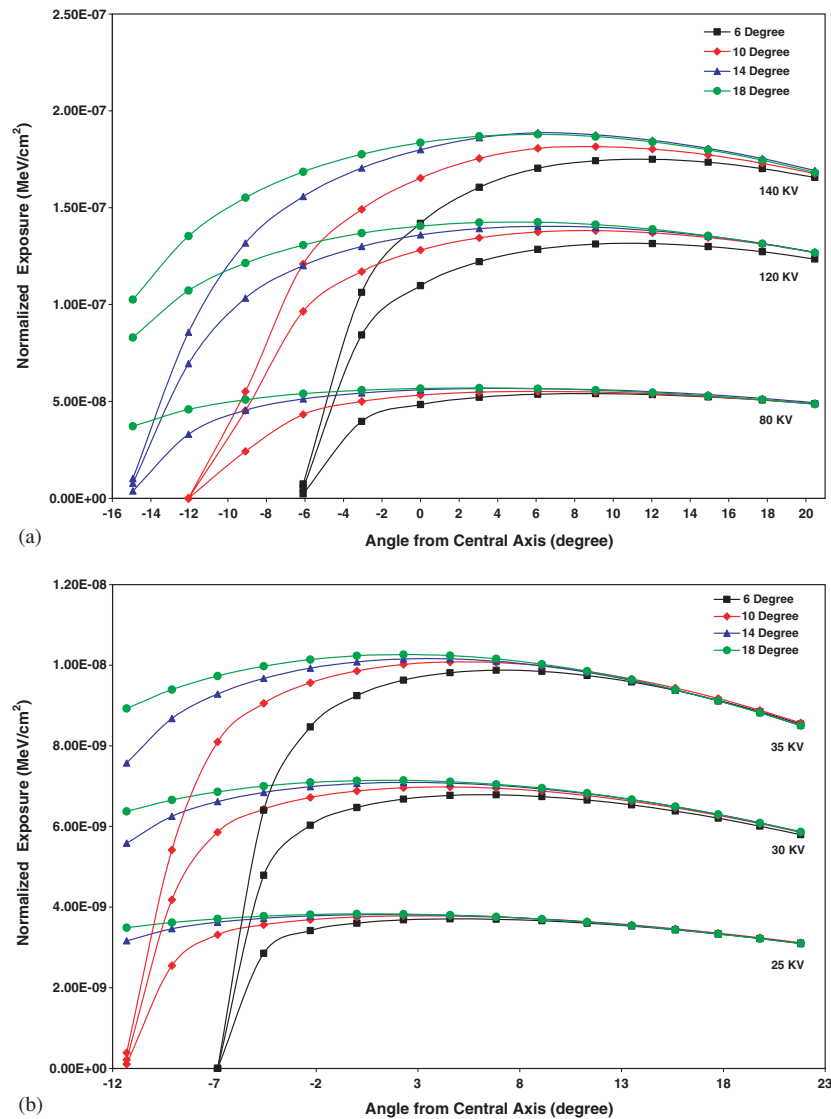


Figure 11. Illustration of anode heel effect for different anode angles for (a) tungsten target with tube voltages between 80 and 140 kV and for (b) molybdenum target with the tube voltages between 25 and 35 kV.

relative exposure on the cathode side is higher than that on the anode side owing to attenuation of the x-ray spectra in the target.

Another problem in x-ray imaging is nonuniformity of exposure in the direction perpendicular to the anode–cathode axis, bearing in mind that the field of view is usually rectangular. Figure 10(c) shows the variation of exposure (normalized to 2×10^7 simulated electrons) on this axis for 8° and 12° target angles at 100 kV tube voltage. The off-axis exposure is identical on both sides of the central axis and the absorption at small target angles is higher than that at large target angles. In addition, we have calculated the off-axis spectra in both cases. The results show that the off-axis and central axis spectra have approximately the same shape without any distortion similar to data shown in figure 9. Our further investigation

Table 3. Variation in radiation exposure for various target angles and tube voltages in the useful x-ray beam.

Tube voltage (kV)	Target material	Difference in radiation exposure in the useful beam ^a (%)			
		Target angle			
		6°	10°	14°	18°
25	Mo	96.0	11.7	3.7	1.3
30	Mo	96.7	15.7	5.7	2.7
35	Mo	97.4	19.8	8.0	4.6
80	W	92.0	21.6	9.5	4.4
120	W	94.2	30.7	14.3	8.4
140	W	94.4	33.2	17.5	11.15

^a From 6° anode side until 6° cathode side.

of the influence of focal spot size on anode heel effect performed by calculating the heel effect for different focal spot sizes (0.3, 0.6, 1.2 mm) indicated that its effect is negligible.

Figure 11(a) shows the anode heel effect for different target angles and tube voltages. The relative difference in radiation exposure in the useful x-ray beam (6° anode side until 6° cathode side) calculated from figure 11(a) is shown in table 3. To demonstrate the validity of results presented in this table, we have compared our simulated data for 12° target angle and 100 kV with experimentally measured and EGS4 Monte Carlo simulation results published by Bhat *et al* (1999). It turns out that the difference in radiation exposure calculated by MCNP4C is 20.5% while this value is 20.0% for EGS4 and 22.0% for measured data (figure 10(a)).

In theory, the anode heel effect is of considerable importance in mammography. It is expected that the conic shape of breasts would require greater radiation intensity near the chest wall rather than to the nipple side so that near uniform exposure of the image receptor will occur. This could be accomplished by positioning the cathode on the chest wall side. However, in practice this is not necessary because compression of the breast ensures that a uniform thickness of tissue is imaged (Bushong 1998). Figure 11(b) shows the anode heel effect for different target angles and tube voltages for Mo/Mo target/filter combinations. The difference in radiation exposure in the useful x-ray beam calculated from figure 11(b) is shown in table 3. It can be seen that the radiation exposure difference in the mammography energy range increases by increasing the tube voltage and decreasing the target angle.

4. Conclusion

Monte Carlo simulation of x-ray spectra has been used extensively in different medical imaging applications including assessment of image quality, optimization of system design and absorbed dose calculation (Caon *et al* 1998, Dance *et al* 2000, Spyrou *et al* 2002, Zaidi and Sgouros 2002). This study used the MCNP4C general-purpose Monte Carlo code for generating x-ray spectra in diagnostic radiology and mammography. Although the simulation of x-ray spectra using the Monte Carlo method is time consuming, the generated x-ray spectra provide detailed information about particles' interaction with different target and filter combinations. This information is useful for x-ray tube design and development of new target/filter combinations to improve image quality in diagnostic radiology and mammography.

The generated x-ray spectra in this work have been verified against IPEM report number 78, experimental measurements and EGS4 Monte Carlo simulations for validation. Although

the paired *t*-test results show no statistically significant differences between simulated and reference spectra, the intensity of characteristic x-rays in MCNP4C simulated spectra is slightly higher than that in IPEM spectra for tube voltages <100 kV, and this behaviour is reversed for tube voltages >100 kV in the diagnostic radiology energy range. Whereas MCNP produces a significantly higher intensity of characteristic x-rays compared to IPEM in mammography when using a Mo target. This discrepancy can be tackled by appropriate adjustment of the XNUM parameter. The results indicate that the MCNP4C general purpose Monte Carlo code with some small adjustment in the appropriate MCNP cards is a useful tool for generating diagnostic radiology and mammography x-ray spectra and investigation of the heel effect.

Acknowledgments

This work was supported by the AmirKabir University of Technology, Department of Physics and Nuclear Sciences and the Swiss National Science Foundation under grant SNSF 3152A0-102143. The authors are indebted to M Bhat for providing measured and EGS4 simulated data.

References

- Acosta E, Liovet X, Coleoni E, Riveros J A and Salvat F 1998 Monte Carlo simulation of x-ray emission by kilovolt electron bombardment *J. Appl. Phys.* **83** 6038–49
- Antonuk L E *et al* 1997 Empirical investigation of the signal performance of a high-resolution, indirect detection, active matrix flat-panel imager (AMFPI) for fluoroscopic and radiographic operation *Med. Phys.* **24** 51–70
- Ay M, Sarkar S, Shahriari M, Sardari D and Zaidi H 2004 Comparative assessment of different computational models for generation of x-ray spectra in diagnostic radiology and mammography *Proc. IEEE Nuclear Science Symposium and Medical Imaging Conference (Rome, Oct 19–22)* at press
- Ben Omrane L, Verhaegen F, Chahed N and Mtimet S 2003 An investigation of entrance surface dose calculations for diagnostic radiology using Monte Carlo simulations and radiotherapy dosimetry formalisms *Phys. Med. Biol.* **48** 1809–24
- Berger M J and Hubbell J H 1987 XCOM: photon cross sections on a personal computer *NBSIR 87-3597* (National Bureau of Standards (US))
- Bhat M, Pattison J, Bibbo G and Caon M 1998 Diagnostic x-ray spectra: a comparison of spectra generated by different computational methods with a measured spectrum *Med. Phys.* **25** 114–20
- Bhat M, Pattison J, Bibbo G and Caon M 1999 Off-axis x-ray spectra: a comparison of Monte Carlo simulated and computed x-ray spectra with measured spectra *Med. Phys.* **26** 303–9
- Birch R and Marshall M 1979 Computation of bremsstrahlung x-ray spectra and comparison with spectra measured with a Ge(Li) detector *Phys. Med. Biol.* **24** 505–17
- Birch R, Marshall M and Ardran G M 1979 Catalogue of spectral data for diagnostic x-rays hospital physicists *Association Scientific Report Series 30*
- Blough M M, Waggener R G, Payne W H and Terry J A 1998 Calculated mammographic spectra confirmed with attenuation curves for molybdenum, rhodium, and tungsten targets *Med. Phys.* **25** 1605–12
- Boone J M 1988 The three parameter equivalent spectra as an index of beam quality *Med. Phys.* **15** 304–10
- Boone J M, Fewell T R and Jennings R J 1997 Molybdenum, rhodium, and tungsten anode spectral models using interpolating polynomials with application to mammography *Med. Phys.* **24** 1863–74
- Boone J M and Seibert J A 1997 An accurate method for computer-generating tungsten anode x-ray spectra from 30 to 140 kV *Med. Phys.* **24** 1661–70
- Briesmeister J F 2000 MCNP—a general Monte Carlo N-particle transport code. version 4C *Los Alamos National Laboratory Report LA-13709-M* (Los Alamos, NM)
- Bushong S C 1998 *Radiologic Science for Technologists: Physics, Biology and Protection* (St. Louis: Mosby Co)
- Caon M, Bibbo G, Pattison J and Bhat M 1998 The effect on dose to computed tomography phantoms of varying the theoretical x-ray spectrum: a comparison of four diagnostic x-ray spectrum calculating codes *Med. Phys.* **25** 1021–7

- Cranley K, Gilmore B J, Fogarty G W A and Desponds L 1997 *IPEM Report 78: Catalogue of Diagnostic X-ray Spectra and Other Data* (CD-Rom Edition 1997) (*Electronic Version prepared by D Sutton*) (York: The Institute of Physics and Engineering in Medicine (IPEM))
- Dance D *et al* 2000 Influence of anode/filter material and tube potential on contrast, signal-to-noise ratio and average absorbed dose in mammography: a Monte Carlo study *Br. J. Radiol.* **73** 1056–67
- Fewell T R and Shuping R E 1977 Photon energy distribution of some typical diagnostic x-ray beams *Med. Phys.* **4** 187–97
- Fewell T R and Shuping R E 1978 *Handbook of Mammography Spectra* (HEW Publication) (FDA) 79-8071
- Fewell T R, Shuping R E and Healy K E 1981 *Handbook of Computed Tomography X-Ray Spectra* (HHS Publication) (FDA) 81-8162 (Washington, DC: US Govt. Printing Office)
- Hughes H G 1997 Status of electron transport in MCNP *Los Alamos National Laboratory LA-UR-97-1368* (Los Alamos, NM)
- ICRU 1989 Tissue Substitutes in Radiation Dosimetry and Measurement *ICRU Report 44* (Bethesda, MD: International Commission on Radiological Units and Measurements (ICRU))
- Kramers H A 1923 On the theory of x-ray absorption and of the continuous x-ray spectrum *Phil. Mag.* **46** 836–71
- Kulkarni R N and Supe S J 1984 Monte Carlo calculations of mammographic x-ray spectra *Phys. Med. Biol.* **29** 185–90
- Laitano R F, Pani R and Pellegrini R 1991 Determination of x-ray spectra and of the scattered component up to 300 kV *Med. Phys.* **18** 934–8
- Mercier J R *et al* 2000 Modification and benchmarking of MCNP for low-energy tungsten spectra *Med. Phys.* **27** 2680–7
- Ng K P, Kwok C S and Tang F H 2000 Monte Carlo simulation of x-ray spectra in mammography *Phys. Med. Biol.* **45** 1309–18
- O'Meara J M, Chettle D R, McNeill F E, Prestwich W V and Svensson C E 1998 Monte Carlo simulation of source-excited *in vivo* x-ray fluorescence measurements of heavy metals *Phys. Med. Biol.* **43** 1413–28
- Pernieka F, Andreo P, Meghziefene A, Czap L and Girzikowsky R 1997 Standards for radiation protection and diagnostic radiology at the IAEA dosimetry laboratory SSDL Newsletter 17 (Vienna: International Atomic Energy Agency)
- Spyrou G, Tzanakos G, Nikiforides G and Panayiotakis G 2002 A Monte Carlo simulation model of mammographic imaging with x-ray sources of finite dimensions *Phys. Med. Biol.* **47** 917–33
- Tucker D M, Barnes G T and Chakraborty D P 1991 Semiempirical model for generating tungsten target x-ray spectra *Med. Phys.* **18** 211–8
- Verhaegen F and Castellano I A 2002 Microdosimetric characterisation of 28 kVp Mo/Mo, Rh/Rh, Rh/Al, W/Rh and Mo/Rh mammography x ray spectra *Radiat. Prot. Dosim.* **99** 393–6
- Verhaegen F, Nahum A E, Van de Putte S and Namito Y 1999 Monte Carlo modelling of radiotherapy kV x-ray units *Phys. Med. Biol.* **44** 1767–89
- Wilkinson L E, Johnston P N and Heggie J C 2001 A comparison of mammography spectral measurements with spectra produced using several different mathematical models *Phys. Med. Biol.* **46** 1575–89
- Zaidi H and Sgouros G (ed) 2002 *Therapeutic Applications of Monte Carlo Calculations in Nuclear Medicine* (Bristol: Institute of Physics Publishing)